Available online at www.sciencedirect.com
ScienceDirect
Journal of Sound and Vibration 307 (2007) 527–544
JOURNAL OF SOUND AND VIBRATION
www.elsevier.com/locate/jsvi

Nonlinear vibration characterization by signal decomposition

P. Frank Pai*

Department of Mechanical and Aerospace Engineering, University of Missouri-Columbia, Columbia, MO 65211, USA

Received 2 June 2005; received in revised form 26 October 2006; accepted 13 June 2007
Available online 28 August 2007

Abstract

Methods for nonlinear vibration characterization by decomposing dynamic responses using the Hilbert–Huang transform and a sliding-window fitting technique are presented. Numerical results show that Hilbert–Huang transform can be used for decomposing nonlinear/non-stationary signals in order to reveal and estimate nonlinear effects. Major nonlinear phenomena that can be extracted from transient and/or steady-state dynamic responses include different nonlinearities, softening and hardening effects, intrawave amplitude- and phase-modulation, distorted harmonic responses under a single-frequency harmonic excitation, interwave amplitude- and phase-modulation, and multiple-mode vibrations caused by internal/external resonances. However, the discontinuity-induced Gibbs' phenomenon makes Hilbert–Huang transform analysis inaccurate around the two data ends. On the other hand, the sliding-window fitting analysis has no Gibbs' phenomenon at the two data ends, but it cannot extract accurate modulation frequencies due to the use of non-orthogonal basis functions in the sliding-window least-squares curve fitting process.

1. Introduction

In the last few decades structural engineers and researchers have been developing dynamics-based methods for rapid damage inspection of large structures [1]. Damage detection is challenging because it is an inverse engineering problem. Based on the complexity of sensor systems used, signal processing methods, and accuracy of deduced damage indicators, dynamics-based damage detection methods can be separated into three groups. Methods in the first group require a simultaneous full-field measurement tool (e.g., Moire interferometry, digital shearography, or scanning laser vibrometers), and they process the measured displacement, slope, or velocity field to compute strains and/or curvatures and then locate damage by examining abnormality or sudden change of these spatially distributed data [2]. Methods in the second group require simultaneous measurements of many points, and they use a well-calibrated structural model and a modal expansion/update method to locate damage. Methods in the third group require simultaneous measurements of only a few locations, and they use the measured time traces and the travelling sequence of abnormality or sudden change in the time traces to locate damage. In-work dynamics-based damage detection methods usually use the third approach. Methods in the first group process spatially distributed data to extract physical variables (such as slopes, curvatures, and strains) to directly reveal damage locations, but the

*Tel.: +1 573 884 1474; fax: +1 573 884 5090.
E-mail address: paip@missouri.edu

0022-460X/$ - see front matter © 2007 Elsevier Ltd. All rights reserved.
doi:10.1016/j.jsv.2007.06.056

challenge is how to extract clear damage indicators from the large amount of data obtained from a full-field measurement. Methods in the second group use the calibrated structural model to compute spatially distributed physical variables to estimate damage locations, but the challenge is how to repeat the same setup conditions used in the structural model and how to correlate the model with currently measured dynamic responses that may be affected by unknown damage and/or changes of physical conditions (such as temperature change, moisture absorption, and changes of boundary conditions). On the other hand, methods in the third group process time-domain data to extract dynamic characteristics (i.e., natural frequencies, damping ratios, and nonlinear effects) to reveal the existence of damage, but the challenge is how to extract linear and nonlinear dynamic characteristics from dynamic responses (especially transient responses) and how to correlate the damage indicators obtained at just a few physical locations to locate damage. Even under small vibrations dynamic responses of damaged structures are often nonlinear because of damage, such as the opening and closing of cracks. This paper presents methods for processing transient and/or steady-state time signals to extract time-varying dynamic characteristics that can be used to reveal damage.

A linear dynamic system has constant natural frequencies, and it vibrates at the frequency of an externally applied harmonic excitation. On the other hand, a nonlinear system has amplitude-dependent natural frequencies, and it may vibrate at a frequency different from an externally applied harmonic excitation. Other nonlinear phenomena include multiple-harmonic response under a single-frequency harmonic excitation, intrawave amplitude- and phase-modulated motions, and multiple-mode vibrations caused by modal interaction (i.e., interwave modulation) [3,4]. One major method for dynamics characterization of a nonlinear system is to examine the harmonic components contained in the system's response to a harmonic excitation. To show the response of a nonlinear oscillator under a harmonic excitation we consider the following weakly nonlinear system:

$$\ddot{u}+\mu\dot{u}+\omega^2u+\mu_3\dot{u}^3+\alpha_2u^2+\alpha_3u^3+\alpha_4u^4+\alpha_5u^5=F\cos(\Omega t+\gamma), \tag{1a}$$

where $\dot{u}\equiv \mathrm{d}u/\mathrm{d}t$, t is the time, α_i are constants, μ and μ_3 are damping coefficients, F is the excitation amplitude, ω is the linear natural frequency, $\Omega(\approx\omega)$ is the excitation frequency, and γ is the phase angle of the excitation w.r.t. the response. The second-order asymptotic solution can be derived using the method of multiple scales to be [5]

$$\begin{aligned}
&u(t)=\sum_{i=0}^{5}a_i\cos(i\Omega t)+b_3\sin(3\Omega t),\\
&a_0=-\frac{\alpha_2a_1^2}{2\Omega^2}-\frac{3\alpha_4a_1^4}{8\Omega^2},\quad a_2=\frac{\alpha_2a_1^2}{6\Omega^2}+\frac{\alpha_4a_1^4}{6\Omega^2},\quad a_3=\frac{\alpha_3a_1^3}{32\Omega^2}+\frac{5\alpha_5a_1^5}{128\Omega^2},\\
&a_4=\frac{\alpha_4a_1^4}{120\Omega^2},\quad a_5=\frac{\alpha_5a_1^5}{384\Omega^2},\quad b_3=\frac{\mu_3\Omega a_1^3}{32},
\end{aligned} \tag{1b}$$

where a_1 is a function of F, μ, and μ_3 and needs to be obtained by solving the modulation equations derived from perturbation analysis [5]. Eq. (1b) reveals that the nonlinear solution is a periodic function (period $T=2\pi/\Omega$) expanded into multiple harmonics. Because α_5 appears in a_3 and α_4 appears in a_2 and a_0 in Eq. (1b), it indicates that higher-order odd-power nonlinearities will behave like the cubic nonlinearity, and higher-order even-power nonlinearities will behave like the quadratic nonlinearity. However, higher-order nonlinearities will introduce more small-amplitude high-frequency harmonics.

To show an example we consider the following damped Duffing oscillator subjected to a harmonic excitation having a frequency Ω close to the linear natural frequency ω and its second-order asymptotic perturbation solution:

$$\ddot{u}+\mu\dot{u}+\omega^2u+\alpha u^3=F\cos\Omega t,\quad \Omega\approx\omega,$$

$$\begin{aligned}
u(t)&=a\cos(\Omega t-\gamma)+a_3\cos(3\Omega t-3\gamma),\quad a_3\equiv\frac{\alpha a^3}{32\Omega^2}\ll a\\
&=\sqrt{a^2+a_3^2+2aa_3\cos(2\Omega t-2\gamma)}\cos(\Omega t-\gamma+\Theta(t))
\end{aligned}$$

$$\approx \sqrt{a^2+a_3^2}\left(1+\frac{a_3}{a}\cos(2\Omega t-2\gamma)\right)\cos(\Omega t-\gamma+\Theta(t)),$$
$$\Theta(t)\equiv \tan^{-1}\frac{a_3\sin(2\Omega t-2\gamma)}{a+a_3\cos(2\Omega t-2\gamma)}\approx \frac{a_3}{a}\sin(2\Omega t-2\gamma), \tag{2}$$

where μ, α, F, and γ are constants. Because $a \gg a_3$ when α is small, the amplitude consists of a constant plus a small amplitude varying at a frequency 2Ω, and the Θ is a small angle varying at a frequency 2Ω. In other words, it is a distorted harmonic with intrawave frequency- and amplitude-modulation caused by nonlinearities. This phenomenon can be used to identify cubic nonlinearity. However, the challenge is how to extract time-varying frequencies of amplitudes and phases from experimental time signals.

To show another example we consider the following nonlinear oscillator with quadratic nonlinearity and its asymptotic perturbation solution:

$$\ddot{u}+\mu\dot{u}+\omega^2u+\alpha u^2=F\cos\Omega t,\quad \Omega\approx\omega,$$

$$u(t)=a_0+a\cos(\Omega t-\gamma)+a_2\cos(2\Omega t-2\gamma),\quad a_2\equiv\frac{\alpha a^2}{6\Omega^2}\ll a$$
$$=a_0+\sqrt{a^2+a_2^2+2aa_2\cos(\Omega t-\gamma)}\cos(\Omega t-\gamma+\Theta(t))$$
$$\approx a_0+\sqrt{a^2+a_2^2}\left(1+\frac{a_2}{a}\cos(\Omega t-\gamma)\right)\cos(\Omega t-\gamma+\Theta(t)),$$
$$\Theta(t)\equiv\tan^{-1}\frac{a_2\sin(\Omega t-\gamma)}{a+a_2\cos(\Omega t-\gamma)}\approx\frac{a_2}{a}\sin(\Omega t-\gamma). \tag{3}$$

Because $a \gg a_2$ when α is small, the amplitude and phase vary at a frequency Ω. In other words, it is a distorted harmonic with intrawave frequency- and amplitude-modulation caused by nonlinearities. This phenomenon can be used to identify quadratic nonlinearity. Again, the problem is how to extract the time-varying frequencies of amplitudes and phases from experimental time signals, especially if only transient data are available.

For a continuous system with certain quadratic nonlinearities, if the dependent variable $w(x,t)$ is discretized using the system's two linear mode shapes $\phi_1(x)$ and $\phi_2(x)$ and the corresponding modal coordinates u_1 and u_2 as

$$w(x,t)=\phi_1(x)u_1(t)+\phi_2(x)u_2(t) \tag{4a}$$

and if the spatial distribution of the excitation force is orthogonal to $\phi_1(x)$, one may obtain the following modal equations:

$$\ddot{u}_1+2\mu_1\omega_1\dot{u}_1+\omega_1^2u_1=u_1u_2,$$
$$\ddot{u}_2+2\mu_2\omega_2\dot{u}_2+\omega_2^2u_2=u_1^2+F\cos\Omega t, \tag{4b}$$

where ω_i are the linear natural frequencies, μ_i are the modal damping ratios, F is the amplitude of the external excitation force, and Ω is the external excitation frequency. The first-order perturbation solution of Eq. (4b) is given as [5]

$$u_1=a_1\cos(\tfrac{1}{2}\Omega t-\tfrac{1}{2}(\gamma_1+\gamma_2)),\quad u_2=a_2\cos(\Omega t-\gamma_2), \tag{4c}$$

where γ_1 and γ_2 are phase angles. It follows from Eq. (4a) that experimental measurement of $w(x,t)$ at any location will consist of u_1 and u_2, which have different characteristic time scales. Then, the challenges are how to separate u_1 and u_2 in order to know the participation of each mode and how to obtain the time-varying frequencies of u_i in order to estimate nonlinearities.

Hence the key for accurate vibration characterization is to decompose complex time signals into functions of different characteristic time scales and extract their time-varying frequencies and amplitudes. This paper investigates the use of Hilbert–Huang transform [6–10] and presents a sliding-window least-squares fitting method for performing such signal decomposition.

2. Signal decomposition methods

Here we present and correlate three signal decomposition methods: the discrete Fourier transform, the Hilbert–Huang transform, and a sliding-window fitting method.

2.1. Discrete Fourier transform

To extract harmonic components from a time signal $u(t)$ the following discrete Fourier transform [11] is usually used:

$$u(k\Delta t) \equiv u_k = a_0 + 2\sum_{i=1}^{N/2}\left(a_i \cos\frac{2\pi i t_k}{T} + b_i \sin\frac{2\pi i t_k}{T}\right) = \text{Real}\left(\sum_{i=-N/2}^{N/2}(a_i - \text{j}b_i)\text{e}^{\text{j}\omega_i t_k}\right), \tag{5a}$$

$$a_0 = \frac{1}{N}\sum_{k=1}^{N} u_k, \quad a_i = \frac{1}{N}\sum_{k=1}^{N} u_k \cos\omega_i t_k, \quad b_i = \frac{1}{N}\sum_{k=1}^{N} u_k \sin\omega_i t_k, \quad \omega_i \equiv 2\pi i/T,$$

$$U(i/T) \equiv a_i - \text{j}b_i = \frac{1}{N}\sum_{k=1}^{N} u_k \text{e}^{-\text{j}\omega_i t_k}, \tag{5b}$$

where $k = 1, \ldots, N$, $\text{j} \equiv \sqrt{-1}$, $t_k \equiv k\Delta t$, Δt is the sampling interval, $1/\Delta t$ is the sampling frequency, N is the total number of samples, T $(= N\Delta t)$ is the sampled period, Δf $(= 1/T)$ is the frequency resolution, and the maximum (Nyquist) frequency is $0.5/\Delta t$ $(= 0.5N/T)$. U is the spectrum of $u(t)$, and a_i and b_i are called spectral coefficients and they represent amplitudes of harmonic components. The expressions of a_i and b_i in Eq. (5a) show that the orthogonality between $u(t)$ and $\cos\omega_i t$ and $\sin\omega_i t$ is used to extract regular harmonics from $u(t)$. Moreover, it is apparent that the time signal $u(t)$ is presented as the summation of $N/2$ harmonics of constant amplitudes and phases. Unfortunately, if $u(t)$ is non-periodic and/or transient, $u(0) \neq u(T)$ and U will include many high-frequency harmonics caused by Gibbs' phenomenon, which makes it difficult to understand $u(t)$ from its spectrum.

2.2. Hilbert–Huang transform

Hilbert–Huang transform is a newly developed technique for processing nonlinear and non-stationary signals [6–10]. The two major steps of Hilbert–Huang transform are (i) using the empirical mode decomposition method to decompose a time-domain signal $u(t)$ into n intrinsic mode functions c_i corresponding to different intrinsic time scales as

$$u(t) = \sum_{i=1}^{n} c_i(t) + r_n, \tag{6}$$

where r_n is the residue, and (ii) performing Hilbert transform and computing the time-dependent frequency ω_i and amplitude A_i of each c_i [6,7]. Then, the time–frequency–energy (i.e., $t - \omega - A$) distribution is named the Hilbert spectrum and is denoted by $H(\omega, t)$.

An intrinsic mode function is a function that satisfies two conditions: (i) the number of extrema and the number of zero crossing must either equal or differ at most by one in the whole data and (ii) the envelope defined by the local maxima and minima is symmetric and hence the mean value of the maxima envelope and the minima envelope is zero at any point. The empirical mode decomposition is based on the assumptions that the signal has at least one maximum and one minimum, and the characteristic time scale is defined by the time lapse between the extrema. Once the extrema are identified, all the local maxima are connected by a natural cubic spline line as the upper envelope. Repeat the procedure for the local minima to produce the lower envelope. The mean of the upper and lower envelopes is designated as m_{11}, and the first intrinsic function is

estimated as c_{11} given by

$$c_{11} = u(t) - m_{11}. \tag{7}$$

Ideally the upper and lower envelopes should cover all the data between them. In reality, overshoots and undershoots may exist, and they generate new extrema and shift or exaggerate the existing ones after the process shown in Eq. (7). New extrema generated in this way actually recover the proper modes lost in the initial examination, and this process can recover low-amplitude riding waves with repeated sifting. This process is like sifting because it uses the characteristic time scale to separate the finest local mode from the data first. The sifting process is to eliminate riding waves and to make the wave-profiles more symmetric. Toward this end, the sifting process has to be repeated more times. In the kth sifting process, c_{1k-1} is treated as the data, then

$$c_{1k} = c_{1k-1} - m_{1k}, \quad k = 2, \ldots, K. \tag{8}$$

Keep repeating the process until all the local maxima are positive, all the local minima are negative, and waves are almost symmetric. Then c_{1k} is accepted as c_1. A systematic method of determining the end of iteration is to limit the deviation D_v computed from the two consecutive sifting results as

$$D_v \equiv \sqrt{\frac{\sum_{i=1}^{N}(c_{1k}(t_i) - c_{1k-1}(t_i))^2}{\sum_{i=1}^{N} c_{1k-1}^2(t_i)}} \tag{9}$$

to be a small number and/or to limit the maximum number of iterations [6,7]. Here $t_i = i\Delta t$ and $N\Delta t = T$ is the sampled period. After the c_1 is obtained, define the residue r_1, treat r_1 as the new data, and repeat the steps shown in Eqs. (7) and (8) as

$$\begin{aligned} &c_{21} = r_1 - m_{21}, \quad r_1 \equiv u(t) - c_1, \\ &c_{2k} = c_{2k-1} - m_{2k}, \quad k = 2, \ldots, K. \end{aligned} \tag{10}$$

After the c_2 is obtained, define the residue r_2, treat r_2 as the new data, and repeat the steps as

$$\begin{aligned} &c_{31} = r_2 - m_{31}, \quad r_2 \equiv u(t) - c_1 - c_2, \\ &c_{3k} = c_{3k-1} - m_{3k}, \quad k = 2, \ldots, K. \end{aligned} \tag{11}$$

The whole sifting process can be stopped when the residue r_n becomes a monotonic function from which no more intrinsic mode function can be extracted. In other words, the last intrinsic mode function has no more than two extrema. For data with a trend, r_n should be the trend. After all $c_i(t)$ are extracted, one can perform Hilbert transform to obtain $d_i(t)$ of each c_i. Then one can define

$$\begin{aligned} &z_i(t) \equiv c_i(t) + \mathrm{j}d_i(t) = A_i \mathrm{e}^{\mathrm{j}\theta_i}, \\ &A_i = \sqrt{c_i^2 + d_i^2}, \quad \theta_i = \tan^{-1} d_i/c_i, \quad \omega_i = \mathrm{d}\theta_i/\mathrm{d}t. \end{aligned} \tag{12}$$

Replacing the $c_i(t)$ in Eq. (6) with the $z_i(t)$ in Eq. (12) and neglecting r_n yields

$$u(t) = \mathrm{Real}\left(\sum_{i=1}^{n} A_i(t)\mathrm{e}^{\mathrm{j}\theta_i(t)}\right), \quad \theta_i(t) = \int_0^t \omega_i(t)\,\mathrm{d}t = \tan^{-1} d_i/c_i. \tag{13}$$

Eqs. (5a) and (13) reveal that the Hilbert–Huang transform (i.e., Eq. (13)) is a generalized Fourier expansion allowing the use of distorted harmonics.

2.2.1. Discussions

The Hilbert–Huang transform is an adaptive method based on the local characteristic time scales of the data under processing. The intrinsic mode functions are usually physical because the characteristic scales are physical. Because distorted harmonics with time-dependent frequencies and amplitudes are allowed in the data decomposition, it does not need spurious harmonics to represent nonlinear/non-stationary signals. Hence, the Hilbert–Huang transform is more appropriate than the Fourier transform [11] and the wavelet transform [12] for signal decomposition and time–frequency–energy presentation of nonlinear/non-stationary signals [6,7].

As shown in Eq. (6), the c_i represent a complete set of basis functions and they are local and adaptive, but they may not be really orthogonal. Even pure harmonics of different frequencies are not exactly orthogonal, and it is why the continuous wavelet in the most commonly used Morlet form suffers severe leakage [12]. However, the empirical mode decomposition used in the Hilbert–Huang transform does not use orthogonality to extract c_i.

The marginal spectrum $h(\omega)(\equiv \int_0^T H(\omega,t)\,\mathrm{d}t)$ from Hilbert–Huang transform analysis offers a measure of total amplitude contribution from each frequency value, and it represents the cumulated amplitude over the entire time span in a probabilistic sense. However, the frequency in $H(\omega,t)$ or $h(\omega)$ has a meaning different from that in Fourier spectra. In Fourier analysis, the existence of energy at a frequency means a regular harmonic wave persisted through the entire time span. In Hilbert–Huang transform analysis, the existence of energy at a frequency only means that, in the entire time span, there is a higher likelihood for such a wave to appear locally. The instantaneous energy density $IE(t)(\equiv \int_0^{1/\Delta t} H^2(\omega,t)\,\mathrm{d}\omega)$ can be used to check the energy fluctuation with time.

2.3. Sliding-window fitting

Several sliding-window fitting methods for time–frequency analysis have been proposed by researchers [13]. Here we use a special set of functions to perform sliding-window fitting in order to show the physical implication of Hilbert–Huang transform, to confirm the accuracy of Hilbert–Huang transform, and to understand the merits and limitations of Hilbert–Huang transform.

If a time signal $u(t)$ is identified from its Fourier spectrum to have two major frequencies ω_1 and $\omega_2(<\omega_1)$, one can assume that

$$\begin{aligned} u(t) &= e_1\cos(\omega_1 t)+e_2\sin(\omega_1 t)+e_3\cos(\omega_2 t)+e_4\sin(\omega_2 t)+e_5+e_6 t \\ &= C_1\cos(\omega_1\bar{t})+\hat{C}_1\sin(\omega_1\bar{t})+C_2\cos(\omega_2\bar{t})+\hat{C}_2\sin(\omega_2\bar{t})+C_3+\hat{C}_3\bar{t}, \end{aligned} \tag{14}$$

where e_i are constants, $\bar{t}(\equiv t-t_s)$ is a moving time coordinate, t_s is the observed instant, and

$$\begin{aligned} &C_1\equiv\sqrt{e_1^2+e_2^2}\cos(\omega_1 t_s-\phi_1), \quad \hat{C}_1\equiv-\sqrt{e_1^2+e_2^2}\sin(\omega_1 t_s-\phi_1), \quad \tan\phi_1\equiv\frac{e_2}{e_1}, \\ &C_2\equiv\sqrt{e_3^2+e_4^2}\cos(\omega_2 t_s-\phi_2), \quad \hat{C}_2\equiv-\sqrt{e_3^2+e_4^2}\sin(\omega_2 t_s-\phi_2), \quad \tan\phi_2\equiv\frac{e_4}{e_3}, \\ &C_3=e_5+e_6 t_s, \quad \hat{C}_3=e_6. \end{aligned} \tag{15}$$

To obtain the coefficients C_j and $\hat{C}_j$ for the data point at $\bar{t}=0$ we use the data points around $t=t_s$ to minimize the square error E_{rror}, which is defined as

$$E_{\mathrm{rror}}\equiv\sum_{i=-m}^{m}\alpha_i(u_i-\bar{u}_i)^2, \tag{16}$$

where u_i denotes $u(\bar{t}_i)$ from Eq. (14) and $\bar{u}_i$ denotes the experimental data at $\bar{t}_i$. The total number of points used is $2m+1$, and α_i is a weighting factor, which can be chosen to be

$$\alpha_i=\frac{1}{1+|\,99i/m\,|}$$

or others. The six equations to determine C_i and $\hat{C}_i$ for the point at $\bar{t}=0$ are given by

$$\frac{\partial E_{\mathrm{rror}}}{\partial C_j}=\sum_{i=-m}^{m}2\alpha_i(u_i-\bar{u}_i)\frac{\partial u_i}{\partial C_j}=0, \quad C_j=C_1,\hat{C}_1,C_2,\hat{C}_2,C_3,\hat{C}_3, \tag{17}$$

which implies that C_j are extracted by using the orthogonality between the functions used in Eq. (14) and the experimental data $\bar{u}_i$. After C_i and $\hat{C}_i$ are determined, it follows from Eq. (14) that

$$u(t_s)=C_1+C_2+C_3. \tag{18}$$

It shows that $u(t_s)$ consists of the "amplitude" C_1 of the harmonic $\cos\omega_1\bar{t}$, the "amplitude" C_2 of the harmonic $\cos\omega_2\bar{t}$, and the moving average C_3. Moreover, it follows from Eq. (15) that

$$A_1 \equiv \sqrt{e_1^2+e_2^2} = \sqrt{C_1^2+\hat{C}_1^2}, \quad \phi_1 = \tan^{-1}\frac{e_2}{e_1} = \omega_1 t_s - \tan^{-1}\frac{-\hat{C}_1}{C_1},$$
$$A_2 \equiv \sqrt{e_3^2+e_4^2} = \sqrt{C_2^2+\hat{C}_2^2}, \quad \phi_2 = \tan^{-1}\frac{e_4}{e_3} = \omega_2 t_s - \tan^{-1}\frac{-\hat{C}_2}{C_2}. \tag{19}$$

If ϕ_1 and ϕ_2 are constant, it follows from Eq. (19) that

$$\omega_1 = \frac{\mathrm{d}\theta_1}{\mathrm{d}t} \approx \frac{\sum_{i=-1}^{2}[\theta_1(t_s+i\Delta t)-\theta_1(t_s+(i-1)\Delta t)]}{4\Delta t},$$
$$\omega_2 = \frac{\mathrm{d}\theta_2}{\mathrm{d}t} \approx \frac{\sum_{i=-1}^{2}[\theta_2(t_s+i\Delta t)-\theta_2(t_s+(i-1)\Delta t)]}{4\Delta t}, \quad \theta_i \equiv \tan^{-1}\frac{-\hat{C}_i}{C_i}. \tag{20}$$

To reduce the influence of noise on calculated ω_i, each ω_i at $t=t_s$ is obtained by averaging over $4\Delta t$, as shown in Eq. (20). The same approach is also used to calculate the ω_i in Eq. (12).

Because harmonic functions are not orthogonal to the polynomial $C_3+\hat{C}_3\bar{t}$, one needs to choose an appropriate window length to enforce the orthogonality in order to obtain unique values for each C_i and $\hat{C}_i$. Numerical results show that an appropriate choice is $2m\Delta t \geqslant 4\pi/\omega_2$, i.e., two periods of the lowest harmonic. This method can be used to extract as many harmonics as needed by adding harmonics identified from the signal's Fourier spectrum to Eq. (14).

3. Nonlinear vibration characterization

As indicated by Eqs. (2), (3) and (5a) that a distorted harmonic is a periodic time signal with intrawave amplitude- and phase-modulation and it can be decomposed into several regular harmonics by discrete Fourier transform analysis. However, perturbation solutions show that nonlinearities cause nonlinear oscillators to have distorted harmonic vibrations under a harmonic excitation. Hence, a distorted harmonic is better than multiple regular harmonics in presenting the response of a nonlinear system to a harmonic excitation. However, the challenge is how to extract quantitative dynamic characteristics and nonlinear effects from dynamic responses, especially if only transient responses are available. Next we demonstrate how to use Hilbert–Huang transform and sliding-window fitting to extract such information from linear, nonlinear, stationary, and/or non-stationary signals.

3.1. Intrawave frequency and amplitude modulation

A steady-state time signal $u(t)$ having a major frequency Ω and an amplitude modulating at a frequency ω can be presented as

$$u(t) = (1+\varepsilon\cos\omega t)\cos\Omega t = \cos\Omega t + \frac{\varepsilon}{2}\cos(\Omega+\omega)t + \frac{\varepsilon}{2}\cos(\Omega-\omega)t, \tag{21}$$

where ε is a small parameter. It reveals that the Fourier spectrum of $u(t)$ from discrete Fourier transform analysis (see Eq. (5b)) will consist a major harmonic (at Ω) with two small harmonics (at $\Omega\pm\omega$) close to it. We note that, if $\omega=0.5\Omega$, $u(t)$ has a period-doubled trajectory on the phase plane $u-\dot{u}$. Moreover, a steady-state time signal $u(t)$ having a major frequency Ω modulating at a frequency ω can be presented as

$$u(t) = \cos(\Omega t+\varepsilon\cos\omega t) \approx (1-\tfrac{1}{4}\varepsilon^2)\cos\Omega t - (\tfrac{1}{2}\varepsilon - \tfrac{1}{16}\varepsilon^3)[\sin(\Omega+\omega)t + \sin(\Omega-\omega)t]$$
$$-\tfrac{1}{8}\varepsilon^2[\cos(\Omega+2\omega)t+\cos(\Omega-2\omega)t] + \tfrac{1}{48}\varepsilon^3[\sin(\Omega+3\omega)t+\sin(\Omega-3\omega)t],$$

$$\hat{\Omega} \equiv \frac{\mathrm{d}(\Omega t+\varepsilon\cos\omega t)}{\mathrm{d}t} = \Omega - \varepsilon\omega\sin\omega t, \tag{22}$$

where Taylor's expansion was performed by treating $\varepsilon\cos\omega t$ as a small variable. Eq. (22) shows that, if $\omega \ll \Omega$, the Fourier spectrum of $u(t)$ consists of several small, uniformly spaced components around Ω. If $\omega \ll \Omega$ and Ω/ω is an irrational number, it is a quasi-periodic motion with a period of infinity. Then, the Fourier spectrum of $u(t)$ contains many extra harmonics due to $u(0) \neq u(T)$, and one may erroneously identify $u(t)$ to be chaotic. Eqs. (21) and (22) clearly show that a distorted harmonic consists of many regular harmonics of small amplitudes.

To show intrawave amplitude- and frequency-modulation we consider the following function:

$$u(t) = (1 + 0.1\cos\omega_a t)\cos(\Omega t + \alpha\sin\omega_p t) + \sigma n(t), \tag{23}$$

where $\Omega = 2\pi$ (i.e., 1 Hz), $\omega_a = 0.1\Omega$, $\omega_p = 0.3\,\Omega$, and $\alpha = 0.5$. $\sigma = 0.004$ and $\Delta t = 0.02$ are used. ($\Delta t = 0.02$ is used in all presented examples, except otherwise stated.) The noise $n(i\Delta t)$, $i = 1, \ldots, 1500$, are obtained using the MATLAB command *randn* and are normally distributed random numbers with a mean zero, a variance one and a standard deviation one. Fig. 1 shows the results from Hilbert–Huang transform and sliding-window fitting analyses, where the thin broken lines in Figs. 1c–f are the original functions in Eq. (23). Figs. 1c–f show that the Hilbert spectra from Hilbert–Huang transform and sliding-window fitting will capture the amplitude-modulation frequency ($\omega_a = 0.1$ Hz), the variation of amplitude ($= \pm 0.1$), the phase-modulation frequency ($\omega_p = 0.3$ Hz), and the variation of frequency ($= \pm\alpha\omega_p = \pm 0.15$ Hz). We note that, for this case, the accuracy of Hilbert spectrum from Hilbert–Huang transform is better than that from sliding-window fitting. It is obvious that the error patterns are different because Hilbert–Huang transform extracts the highest-frequency intrinsic mode function first and the lowest-frequency intrinsic mode function last, but the sliding-window fitting extracts all intrinsic mode functions at the same time. Non-orthogonality of the functions used in Eq. (14) causes leakage errors in sliding-window fitting analysis and the extracted functions may be different from intrinsic mode functions. If $\omega_p = 0.2\Omega$, the errors in the sliding-window fitting become smaller because of function orthogonality.

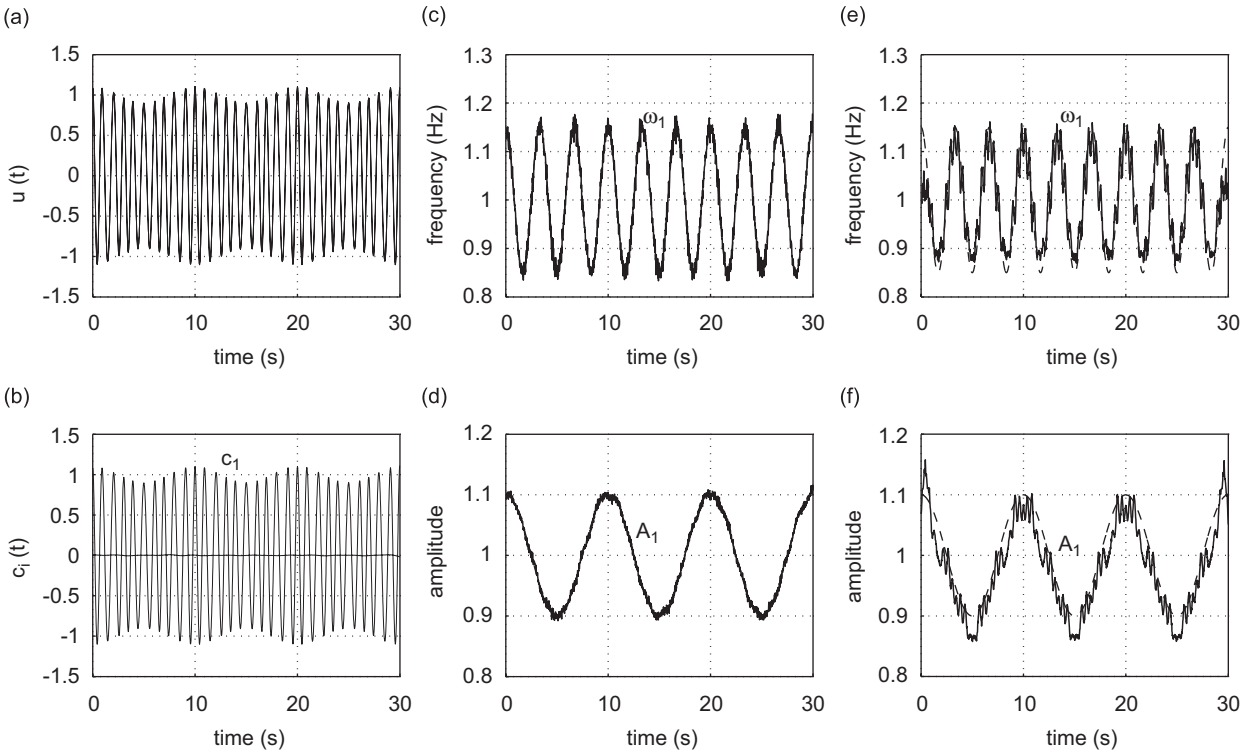

Fig. 1. Hilbert–Huang transform and sliding-window fitting analyses of Eq. (23) with $\omega_a = 0.1\Omega$, $\omega_p = 0.3\Omega$, and $\alpha = 0.5$: (a) $u(t)$, (b) c_1 and r_1, (c) frequency ω_1 of c_1, (d) amplitude A_1 of c_1 from Hilbert–Huang transform, (e) ω_1 of C_1, and (f) A_1 of C_1 from sliding-window fitting.

The cubic spline fitting (affected by noise) of local extrema causes errors in the Hilbert–Huang transform, and the most serious errors of Hilbert–Huang transform occur at the two ends and are mainly caused by discontinuity (due to $c_i(0) \neq c_i(T)$) and hence Gibbs' phenomenon induced during the Hilbert transform of each intrinsic mode function. To reduce Gibbs' phenomenon in the Hilbert transform of an intrinsic mode

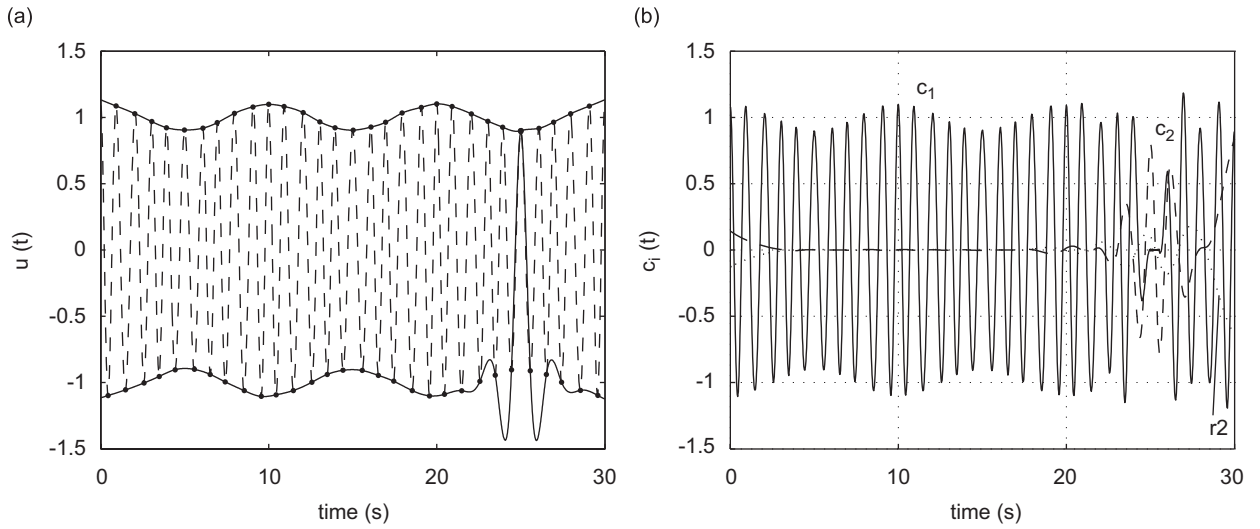

Fig. 2. Hilbert–Huang transform of Eq. (23) with $\text{itr}_{\max} = 5$: (a) the first set of upper and lower envelopes and (b) c_1, c_2, and r_2 (dots).

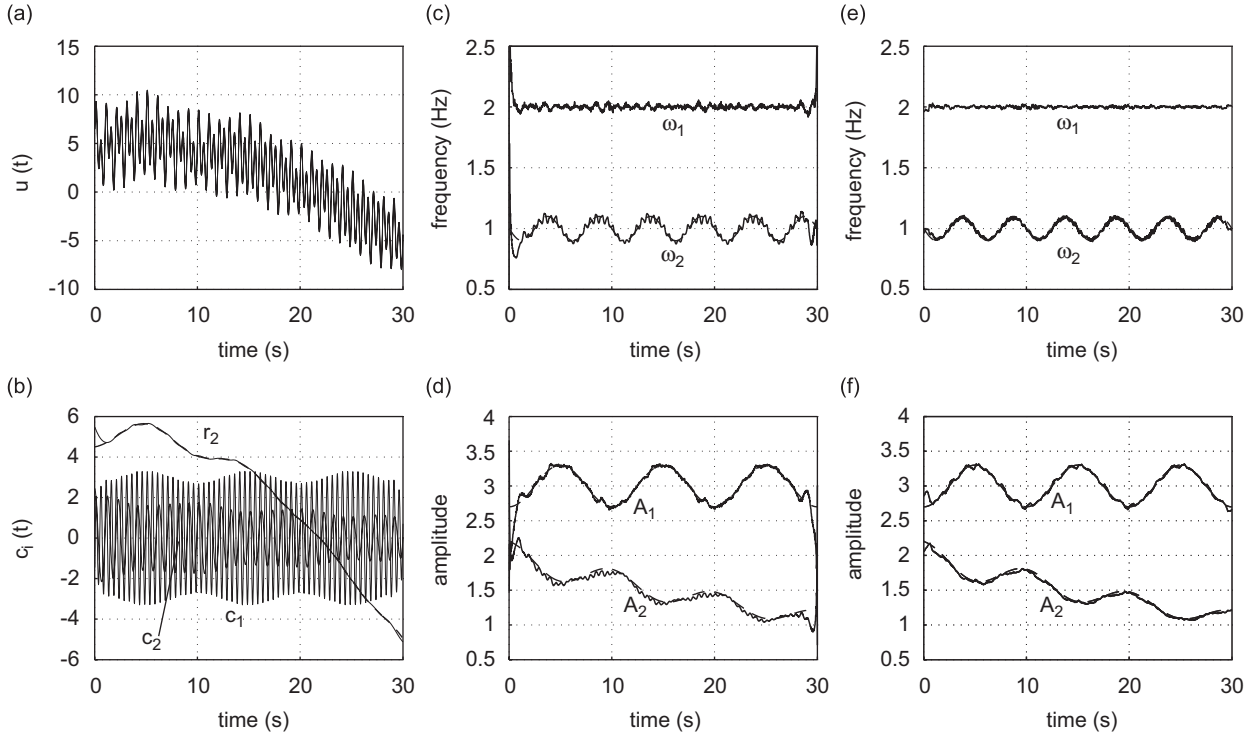

Fig. 3. Hilbert–Huang transform and sliding-window fitting analyses of Eq. (24) with $\omega_a = 0.1\Omega$, $\omega_p = 0.2\Omega$, and $\alpha = 0.5$: (a) $u(t)$, (b) c_i and r_2, (c) frequencies ω_i of c_i, (d) amplitudes A_i of c_i from Hilbert–Huang transform, (e) ω_i of C_i, and (f) A_i of C_i from sliding-window fitting.

function, one can add to the two ends characteristic waves to make the slightly enlarged data begin and end with zero. However, because it is not a systematic approach, it is not exercised in any of the presented examples. The c_1 in Fig. 1b is obtained using $\text{itr}_{\max} = 20$ (the maximum allowable number of iterations) and $D_v = 0.001$. If $\text{itr}_{\max} = 5$ and/or a different set of $n(i\Delta t)$ are used, Fig. 2 shows that Hilbert–Huang transform fails because the noise creates extra local extrema and messes up the cubic spline fitting, and the extracted functions may be misunderstood as intermittent signals, as shown in Fig. 2b. We also note that, when $\text{itr}_{\max}$ increases, the Gibbs' phenomenon becomes more serious but more localized at the two ends. Fig. 2b also shows that, if $u(t)$ is really intermittent, one intrinsic mode function could contain two time scales and the neighboring intrinsic mode functions might contain oscillations of the same scale. However, signals of the same time scale would never occur at the same location in two different intrinsic mode functions.

Next we perform Hilbert–Huang transform and sliding-window fitting analyses of the following function:

$$u(t) = (1 - 0.1\cos\omega_a t)(3\sin(2\Omega t) + 5 + 0.1t - 0.015t^2) + 2(1 + 0.1\cos\omega_a t)e^{-0.02t}\sin(\Omega t + \alpha\cos\omega_p t) + \sigma n(t), \tag{24}$$

where $\Omega = 2\pi$, $\omega_a = 0.1\Omega$, $\omega_p = 0.2\Omega$, $\alpha = 0.5$, $\sigma = 0.01$, and $\Delta t = 0.02$. Fig. 3 shows the results, where the broken thin lines represent the original functions in Eq. (24). We note that the Hilbert spectra from Hilbert–Huang transform and sliding-window fitting have about the same level of accuracy, and both well capture the amplitude-modulation frequency ($\omega_a = 0.1$ Hz), the variations of amplitudes ($= \pm 0.1A_i$), the phase-modulation frequency ($\omega_p = 0.2$ Hz), the variation of frequency ($= \pm\alpha\omega_p = \pm 0.1$ Hz), and the low-frequency transient part (i.e., r_2 and C_3 (not shown)). Again, Gibbs' phenomenon causes errors at the two ends of A_i and ω_i from Hilbert–Huang transform analysis.

If $u(t) = \cos(\Omega + \varepsilon)t + \cos(\Omega - \varepsilon)t$, it is an amplitude-modulated function with an average amplitude of zero because $u(t) = 2\cos(\varepsilon t)\cos(\Omega t)$. Unfortunately, because the Hilbert–Huang transform procedure implicitly confines the amplitudes of c_i to be positive, Hilbert–Huang transform will extract from $u(t)$ only one

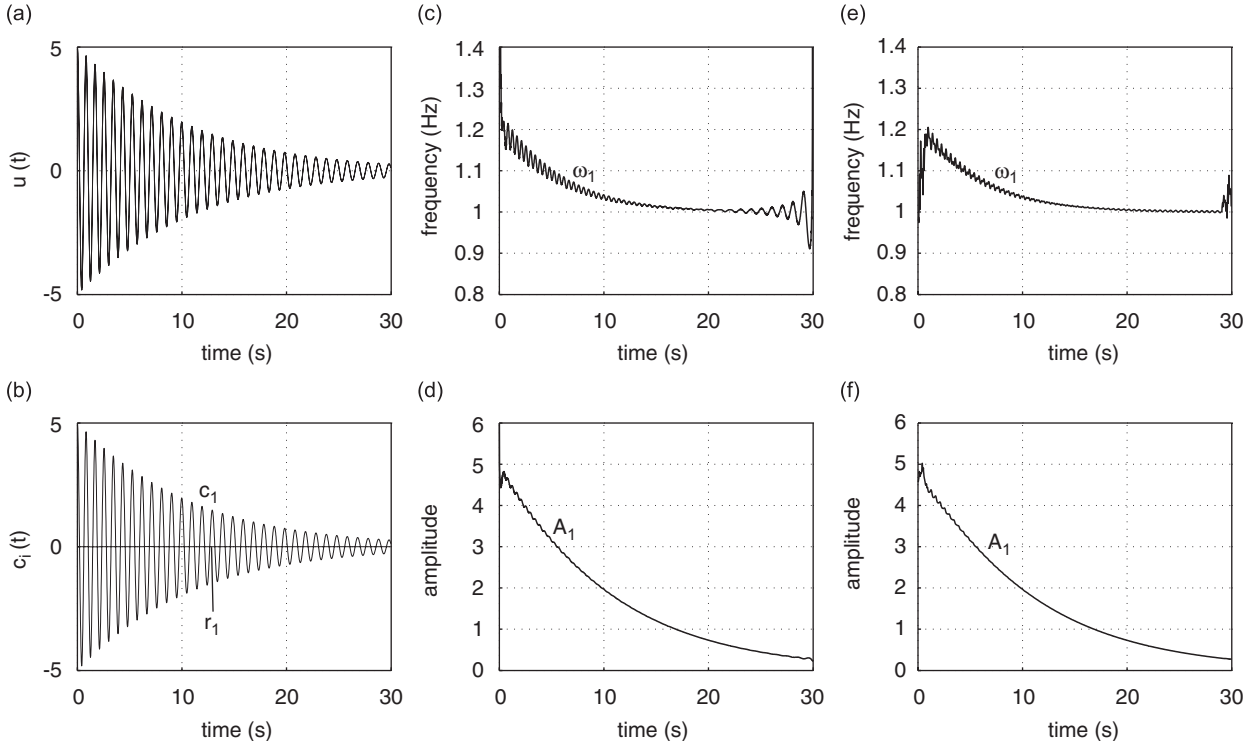

Fig. 4. Hilbert–Huang transform and sliding-window fitting analyses of Eq. (25) with $F = 0$, $\alpha = 1$, $u(0) = 5$, and $\dot{u}(0) = 0$: (a) $u(t)$, (b) c_1 and r_1, (c) frequency ω_1 of c_1, (d) amplitude A_1 of c_1 from Hilbert–Huang transform, (e) ω_1 of C_1, and (f) A_1 of C_1 from sliding-window fitting.

amplitude-modulated intrinsic mode function with a varying frequency at locations where A_1 (>0) is close to zero. For such cases, Fourier transform produces the best results because the data are linear and stationary.

3.2. Different nonlinearities

3.2.1. Cubic nonlinearity

We consider the following oscillator with cubic nonlinearity:

$$\ddot{u} + 0.2\dot{u} + (2\pi)^2 u + \alpha u^3 = F\cos(\Omega t). \tag{25}$$

For a free damped vibration with $F = 0$, $\alpha = 1$, $u(0) = 5$, and $\dot{u}(0) = 0$, Fig. 4 shows the results of Hilbert–Huang transform and sliding-window fitting analyses. The Hilbert spectrum from Hilbert–Huang transform (i.e., Figs. 4c and d) reveals that the natural frequency ω_1 is about 1 Hz and the amplitude- and frequency-modulation frequency $\omega_p = 2\omega_1$, which indicates the nonlinearity is cubic, as shown by Eq. (2). Moreover, because ω_1 increases when the amplitude A_1 increases, it is a hardening nonlinearity (i.e., $\alpha>0$) because $\omega_1 = \omega_0 + 3\alpha A_1^2/(8\omega_0)$ ($\omega_0 = 2\pi$) from perturbation analysis [5]. The α can be reasonably estimated using the perturbation solution as $\alpha = 8\omega_0(\omega_1 - \omega_0)/(3A_1^2)$. We note that the Hilbert spectrum from sliding-window fitting also indicates $\omega_p = 2\omega_1$ but it is not clear because of leakage errors caused by function non-orthogonality.

For a forced vibration with $F = 5$, $\alpha = -1$, $\Omega = \pi$, $u(0) = 4$, and $\dot{u}(0) = 0$, Fig. 5 shows the results from Hilbert–Huang transform and sliding-window fitting analyses. It is obvious that c_1 is the distorted, damped natural harmonic, c_2 is the distorted harmonic caused by the excitation at $\Omega = 0.5$ Hz and the cubic nonlinearity, and r_2 is the lowest-frequency harmonic representing the trend (i.e., the moving average) of the signal and is about zero for this case. Figs. 5c and d clearly show that the frequency of c_1 modulates at $2\omega_1$ when A_1 is large, and the frequency of c_2 modulates at 1 Hz ($= 2\Omega$) because of the cubic nonlinearity.

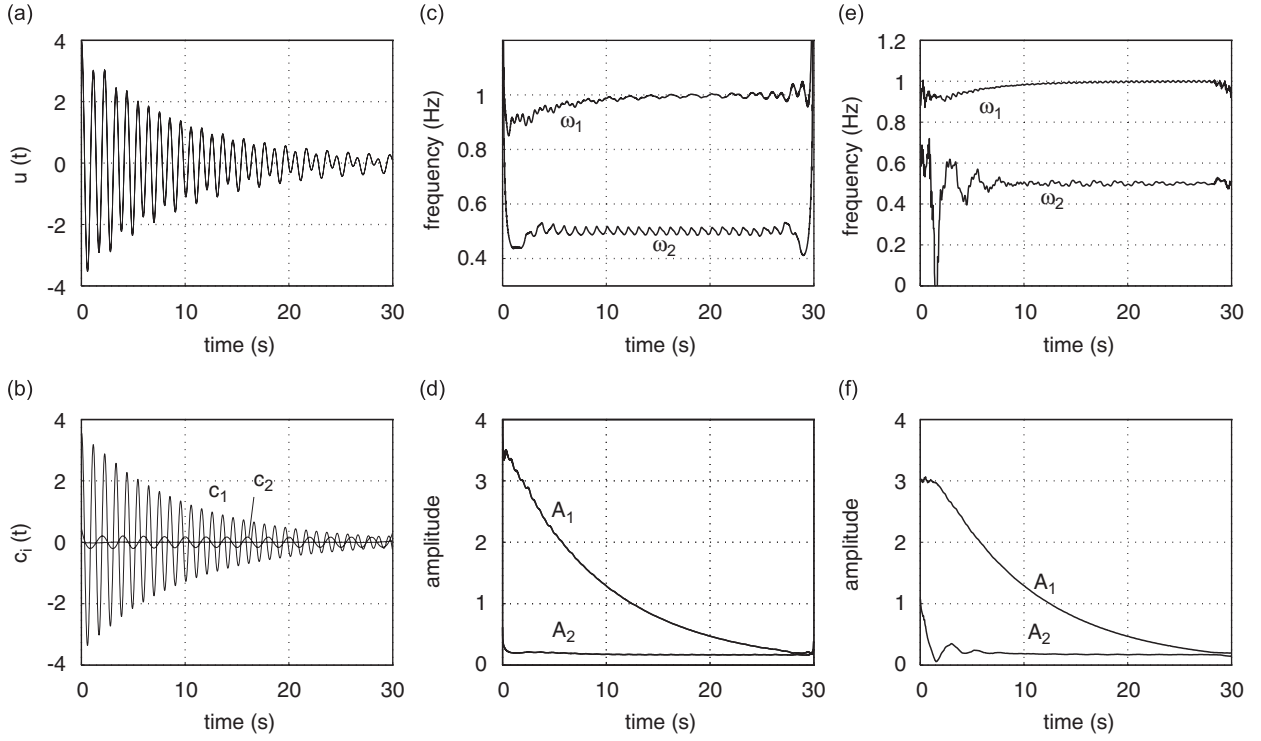

Fig. 5. Hilbert–Huang transform and sliding-window fitting analyses of Eq. (25) with $F = 5$, $\alpha = -1$, $\Omega = \pi$, $u(0) = 4$, and $\dot{u}(0) = 0$: (a) $u(t)$, (b) c_i and r_2, (c) frequencies ω_i of c_i, (d) amplitudes A_i of c_i from Hilbert–Huang transform, (e) ω_i of C_i, and (f) A_i of C_i from sliding-window fitting.

Moreover, because ω_1 decreases when the amplitude A_1 increases, it is a softening cubic nonlinearity (i.e., $\alpha<0$). We note that the Hilbert spectrum from sliding-window fitting (see Figs. 5e and f) cannot show the correct modulation frequency because the fixed value assigned to the ω_1 in Eq. (14) is obtained from the Fourier spectrum of discrete Fourier transform analysis and it cannot cope with the significant variation of ω_1 shown in Fig. 5c. Hence, the non-orthogonality causes leakage errors in sliding-window fitting analysis and the spectrum is wrong, especially ω_2 and A_2. The spectra from the wavelet analysis or the discrete Fourier transform analysis consist of 0.5, 1.0, and 1.5 Hz harmonics and many other higher harmonics caused by transient effects, instead of just two intrinsic mode functions. It is obvious that Hilbert–Huang transform can extract transient and steady-state harmonics (distorted or not) of different time scales and reveal nonlinearities from non-stationary data without dealing with the higher harmonics caused by transient effects.

3.2.2. *Quadratic nonlinearity*

Next we consider the following oscillator with quadratic nonlinearity:

$$\ddot{u}+0.2\dot{u}+(2\pi)^2u+\alpha u^2=F\cos(\Omega t). \tag{26}$$

For a free damped vibration with $F=0$, $\alpha=1$, $u(0)=5$, and $\dot{u}(0)=0$, Fig. 6 shows the results of Hilbert–Huang transform and sliding-window fitting analyses. Fig. 6c reveals that the natural frequency ω_1 is about 1 Hz and the frequency-modulation frequency $\omega_p=\omega_1$, which indicates that the nonlinearity is quadratic, as shown by Eq. (3). Moreover, it shows that ω_1 decreases when the amplitude A_1 increases, as predicted by the perturbation solution $\omega_1=\omega_0-5\alpha^2A_1^2/(12\omega_0^3)$ ($\omega_0=2\pi$) [5]. The α can be reasonably estimated using the perturbation solution as $\alpha=\sqrt{12\omega_0^3(\omega_0-\omega_1)/(5A_1^2)}$. Moreover, the expression of a_0 in Eq. (1b) indicates that $\alpha>0$ because $r_1(t)<0$, as shown in Fig. 6b. We note that the Hilbert spectrum from sliding-window fitting also shows the softening effect but it does not clearly indicate $\omega_p=\omega_1$ due to leakage errors caused by non-orthogonality of the functions used in Eq. (14).

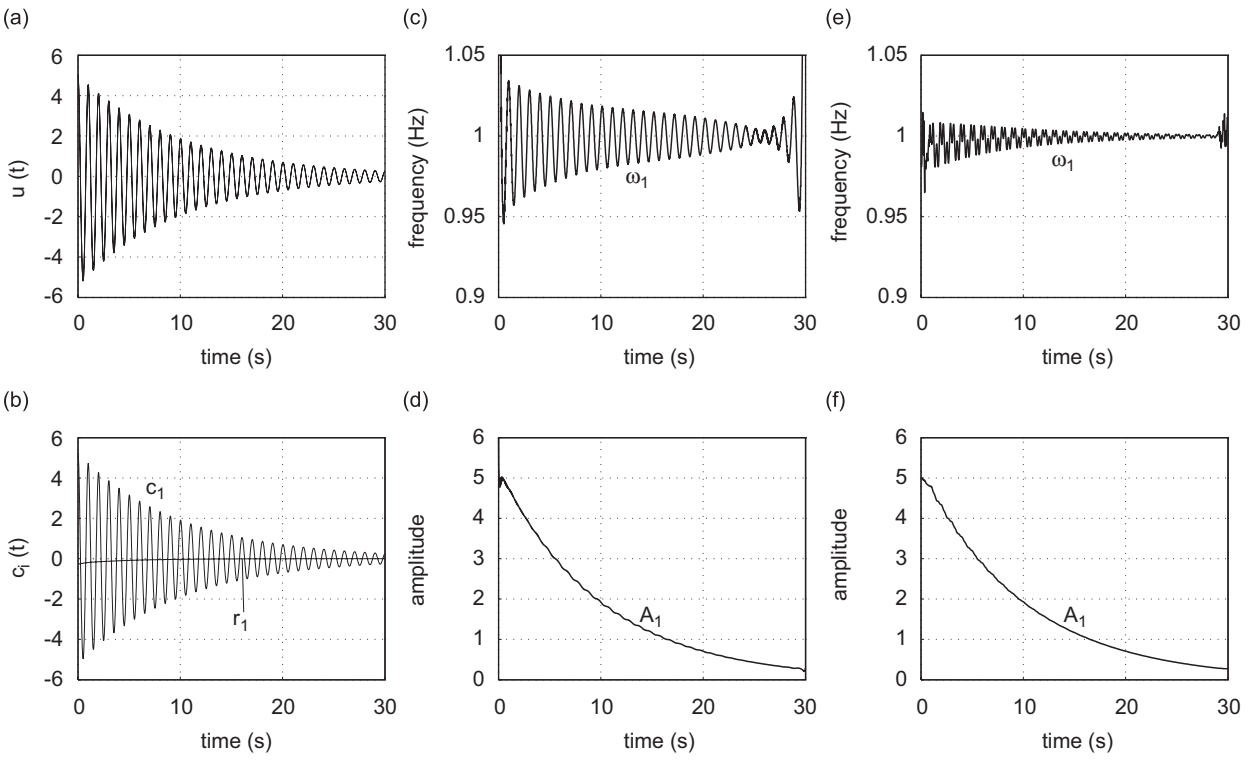

Fig. 6. Hilbert–Huang transform and sliding-window fitting analyses of Eq. (26) with $F=0$, $\alpha=1$, $u(0)=5$, and $\dot{u}(0)=0$: (a) $u(t)$, (b) c_1 and r_1, (c) ω_1 of c_1, (d) A_1 of c_1 from Hilbert–Huang transform, (e) ω_1 of C_1, and (f) A_1 of C_1 from sliding-window fitting.

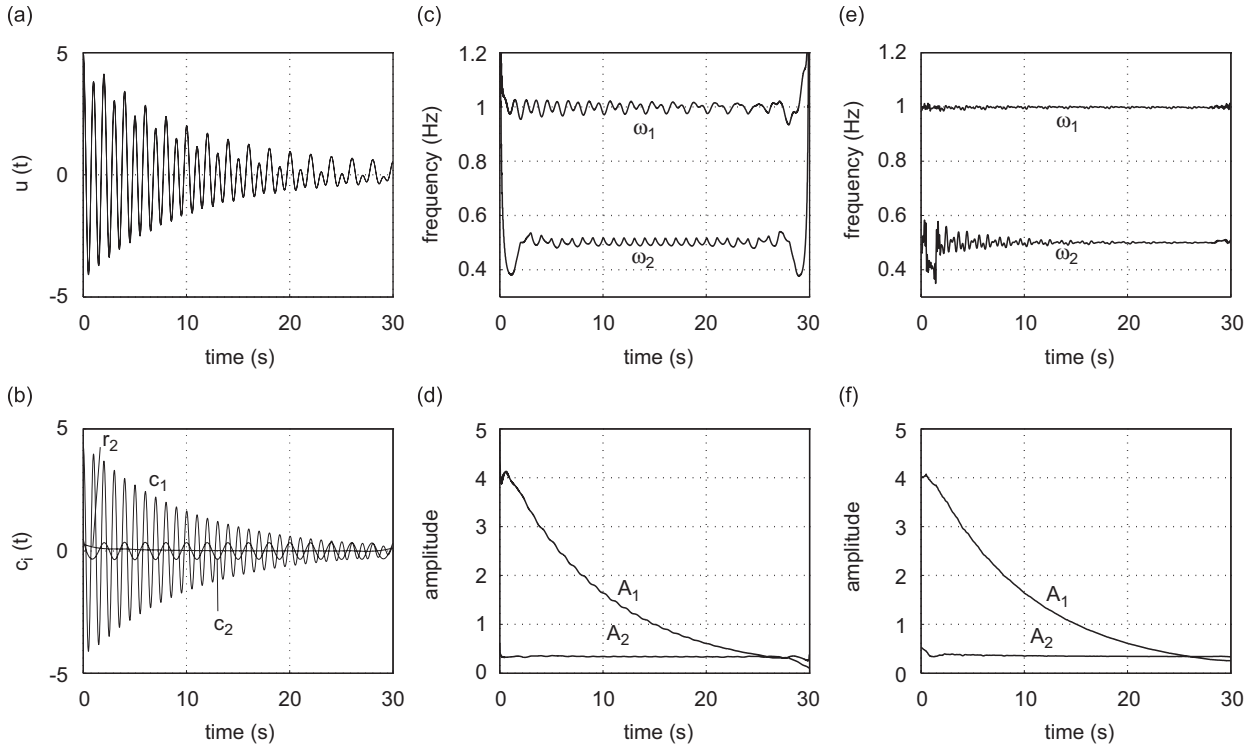

Fig. 7. Hilbert–Huang transform and sliding-window fitting analyses of Eq. (26) with $F = 10$, $\alpha = -1$, $\Omega = \pi$, $u(0) = 5$, and $\dot{u}(0) = 0$: (a) $u(t)$, (b) c_i and r_2, (c) ω_i of c_i, (d) A_i of c_i from Hilbert–Huang transform, (e) ω_i of C_i, and (f) A_i of C_i from sliding-window fitting.

For a forced vibration with $F = 10$, $\alpha = -1$, $\Omega = \pi$, $u(0) = 5$, and $\dot{u}(0) = 0$, Fig. 7 shows the results of Hilbert–Huang transform and sliding-window fitting analyses. Fig. 7c shows that c_1 is the distorted, damped natural harmonic, c_2 is the distorted harmonic caused by the excitation at $\Omega = 0.5$ Hz and the quadratic nonlinearity, and r_2 is the lowest-frequency harmonic representing the trend (i.e., the moving average) of the signal. Fig. 7c clearly shows that, because of the quadratic nonlinearity, the frequency of c_1 modulates at ω_1 when A_1 is large. Moreover, because $r_2 > 0$, it follows from the a_0 shown in Eq. (1b) that $\alpha < 0$. We note that the Hilbert spectrum from sliding-window fitting does not clearly reveal the modulation frequencies due to leakage errors caused by non-orthogonality.

3.2.3. Higher-order nonlinearities

To show the effects of higher-order nonlinearities, we consider the following oscillator:

$$\ddot{u} + 0.2\dot{u} + (2\pi)^2 u + \alpha u^5 = 0. \tag{27}$$

For a free damped vibration with $\alpha = 1$, $u(0) = 5$, and $\dot{u}(0) = 0$, Fig. 8 shows the results of Hilbert–Huang transform analysis. The Hilbert spectrum reveals that the natural frequency ω_1 significantly changes with the amplitude A_1 and the amplitude- and frequency-modulation frequency is $2\omega_1(t)$, like cubic nonlinearity. The a_3 in Eq. (1b) being a function of α_5 implies that higher-order odd-power nonlinearities behave like cubic nonlinearity. Moreover, $r_1(t) = 0$ and the modulation waves of $\omega_1(t)$ and $A_1(t)$ are found to be distorted harmonics (see Figs. 8e and f), which imply that the power of nonlinearity is odd and higher than 3. Because ω_1 increases when the amplitude A_1 increases, it is a hardening nonlinearity (i.e., $\alpha > 0$) because $\omega_1 = \omega_0 + 5\alpha A_1^4/(16\omega_0)$ ($\omega_0 = 2\pi$) from perturbation analysis [5]. The α can be estimated using the perturbation solution as $\alpha = 16\omega_0(\omega_1 - \omega_0)/(5A_1^4)$. We note that the sliding-window fitting analysis cannot work for this case because it has a wide frequency band, as shown by Fig. 8c.

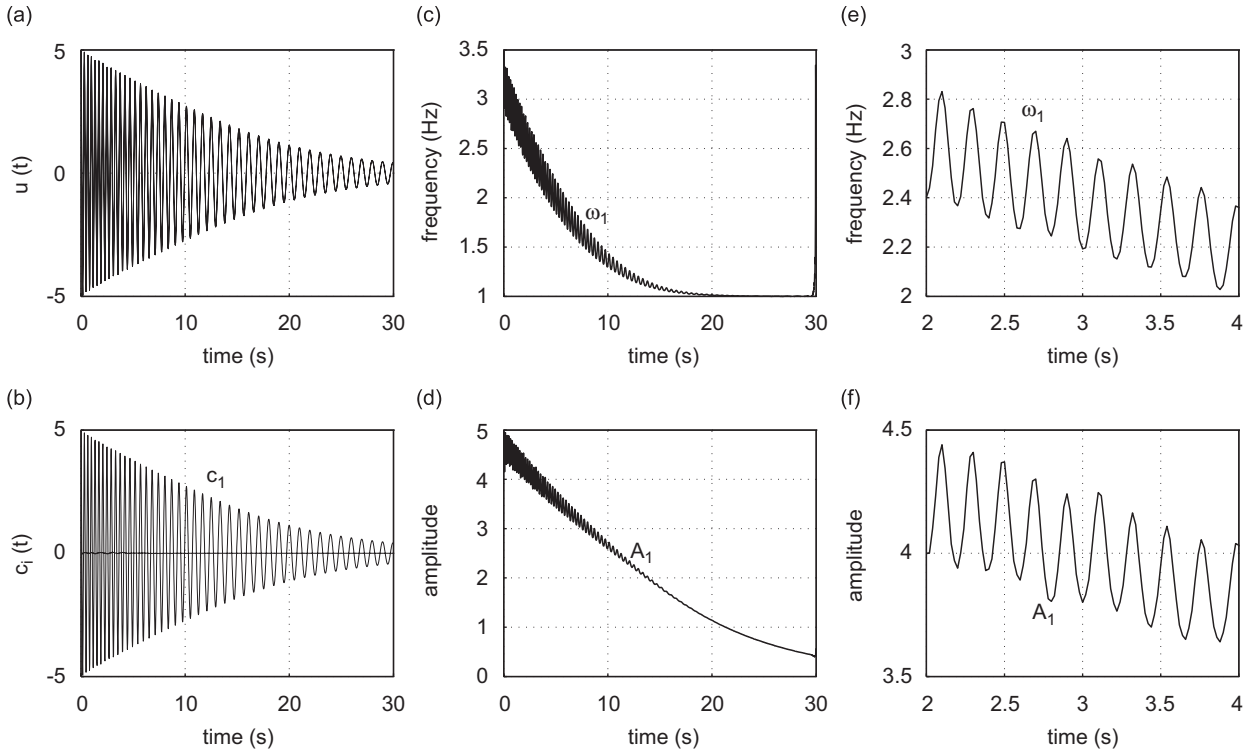

Fig. 8. Hilbert–Huang transform analysis of Eq. (27) with $\alpha = 1$, $u(0) = 5$, and $\dot{u}(0) = 0$: (a) $u(t)$, (b) c_1 and r_1, (c) ω_1 of c_1, (d) A_1 of c_1, (e) ω_1 of c_1, and (f) A_1 of c_1.

3.3. Interwave frequency and amplitude modulation

Next we consider the following quadratically coupled nonlinear oscillator:

$$\ddot{u}_1 + 0.05\dot{u}_1 + (2\pi)^2 u_1 = 20u_1u_2,$$
$$\ddot{u}_2 + 0.05\dot{u}_2 + (4\pi)^2 u_2 = 20u_1^2. \tag{28}$$

For a free damped vibration with $u_1(0) = 1$, $\dot{u}_1(0) = 0$, $u_2(0) = -1$, and $\dot{u}_2(0) = 0$, Figs. 9 and 10 show the Hilbert–Huang transform analysis of $u_1(t)$ and $u_2(t)$, respectively. Fig. 9b shows that u_1 behaves like $u_1 = A_1(t)\cos\omega_1 t$. Because $u_1^2 = 0.5A_1^2(1 + \cos 2\omega_1 t)$, the drift term $r_1(t)(>0)$ of u_2 in Fig. 10b is due to this transient excitation $0.5A_1^2(t)$ from u_1^2. Because Fig. 10b shows that u_2 behaves like u_1^2 and hence $20u_1u_2$ is like a cubic nonlinearity to u_1 (see Eq. (28)), it causes the 2 Hz ($= 2\omega_1$) modulation of ω_1 and A_1 in Figs. 9c and d. The 0.2 Hz modulation in Figs. 9d and 10d is caused by the coupling of u_1 and u_2 and is determined by the coupling nonlinearities and damping coefficients. If only $u_1 + u_2$ can be measured in the actual situation (see Eq. (4a)), Fig. 11 shows the results of Hilbert–Huang transform and sliding-window fitting analyses. Fig. 11c shows that the interwave modulation between u_1 ($= c_2$) and u_2 ($= c_1$) messes up the distributions of extrema (see Figs. 11a and 2a) and hence the Hilbert spectrum from Hilbert–Huang transform is less accurate than that from sliding-window fitting analysis. The sliding-window fitting analysis is more appropriate for extracting intrinsic mode functions with constant frequencies.

3.4. Discussions

The presented methods of extracting nonlinear phenomena can be used for structural damage detection because damaged structures often behave nonlinearly even under small vibrations. For example, the opening and closing of cracks in a structure may cause frequency- and amplitude-modulations and/or localized

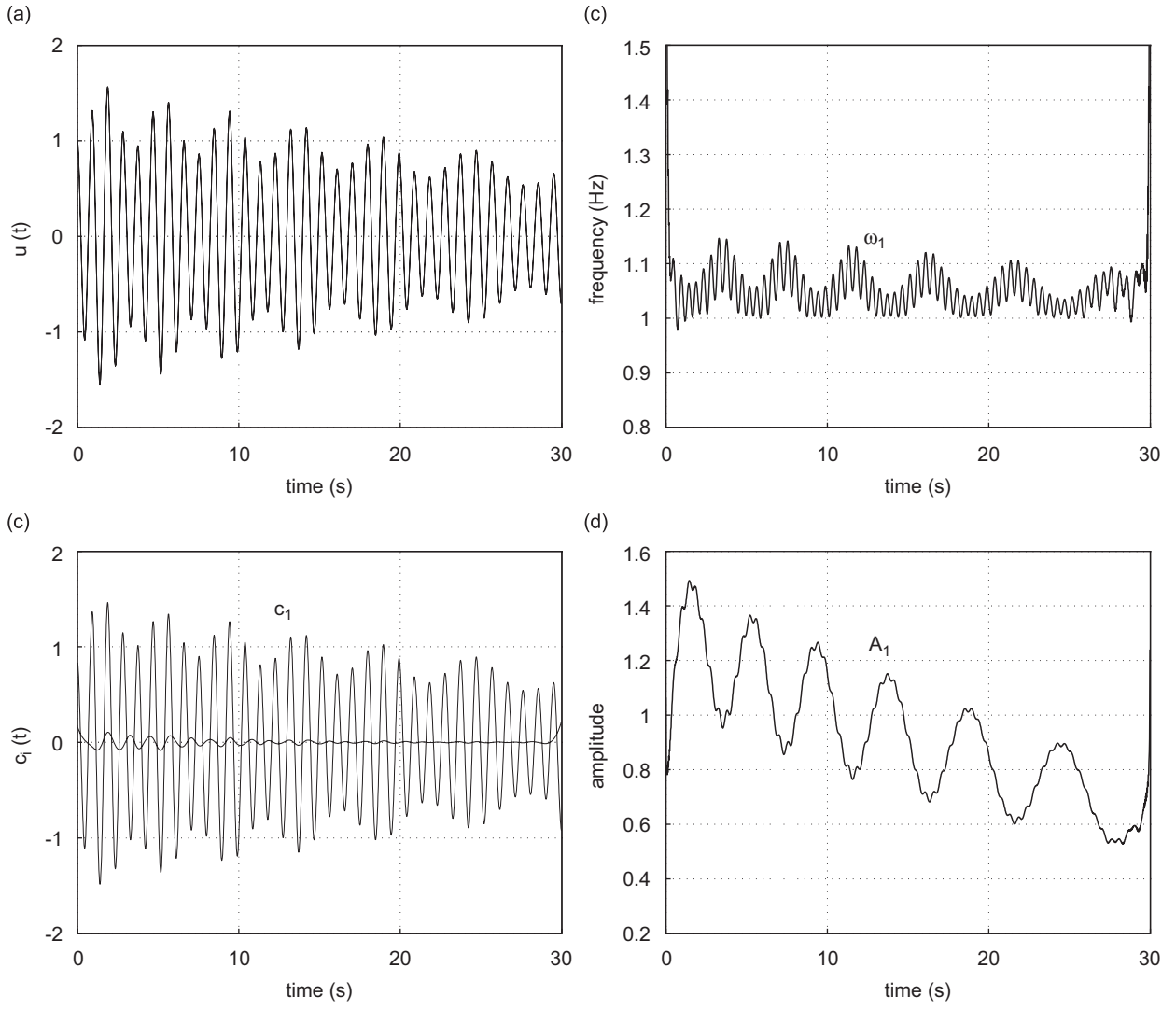

Fig. 9. Hilbert–Huang transform analysis of $u(t)$ $(= u_1(t))$ of Eq. (28): (a) $u_1(t)$, (b) c_1 and r_1, (c) ω_1 of c_1, and (d) A_1 of c_1.

transient vibration. In Hilbert–Huang transform analysis, because m_{ik} is the average of the upper and lower cubic spline envelopes, m_{ik}, $\dot{m}_{ik}$ and $\ddot{m}_{ik}$ are continuous time functions. Consequently, the discontinuities of u, $\dot{u}$, and $\ddot{u}$ remain in $c_1(t)$ (see Eq. (7)) and the discontinuities of third-order and other higher-order time derivatives of u are shared by all extracted c_i and r_n. Hence, one can process $c_1(t)$, instead of the original data $u(t)$, in using structural damage detection methods based on the use of discontinuities of u, $\dot{u}$, and $\ddot{u}$. Hence Hilbert–Huang transform can be used for processing any transient and/or steady-state time signals to extract time-varying dynamic characteristics to reveal damage in structures. The use of Hilbert–Huang transform for structural damage detection will be reported separately [14].

The presented signal decomposition method is different from the conventional frequency tracking method in the literature. The frequency tracking method is usually for on-line estimation of the major frequency of the incoming signal for some applications that may not have access to blocked data and thus require continuously updating frequency estimates. The applications include decoding digital information from a frequency-shift keyed bit stream, demodulation of an FM radio signal, tracking the engine speed of a maneuvering vessel via acoustic data, pitch-tracking in speech and music, and modeling of vibrato (frequency modulation) in music performance. The presented method is more for system identification by decomposing a set of recorded block

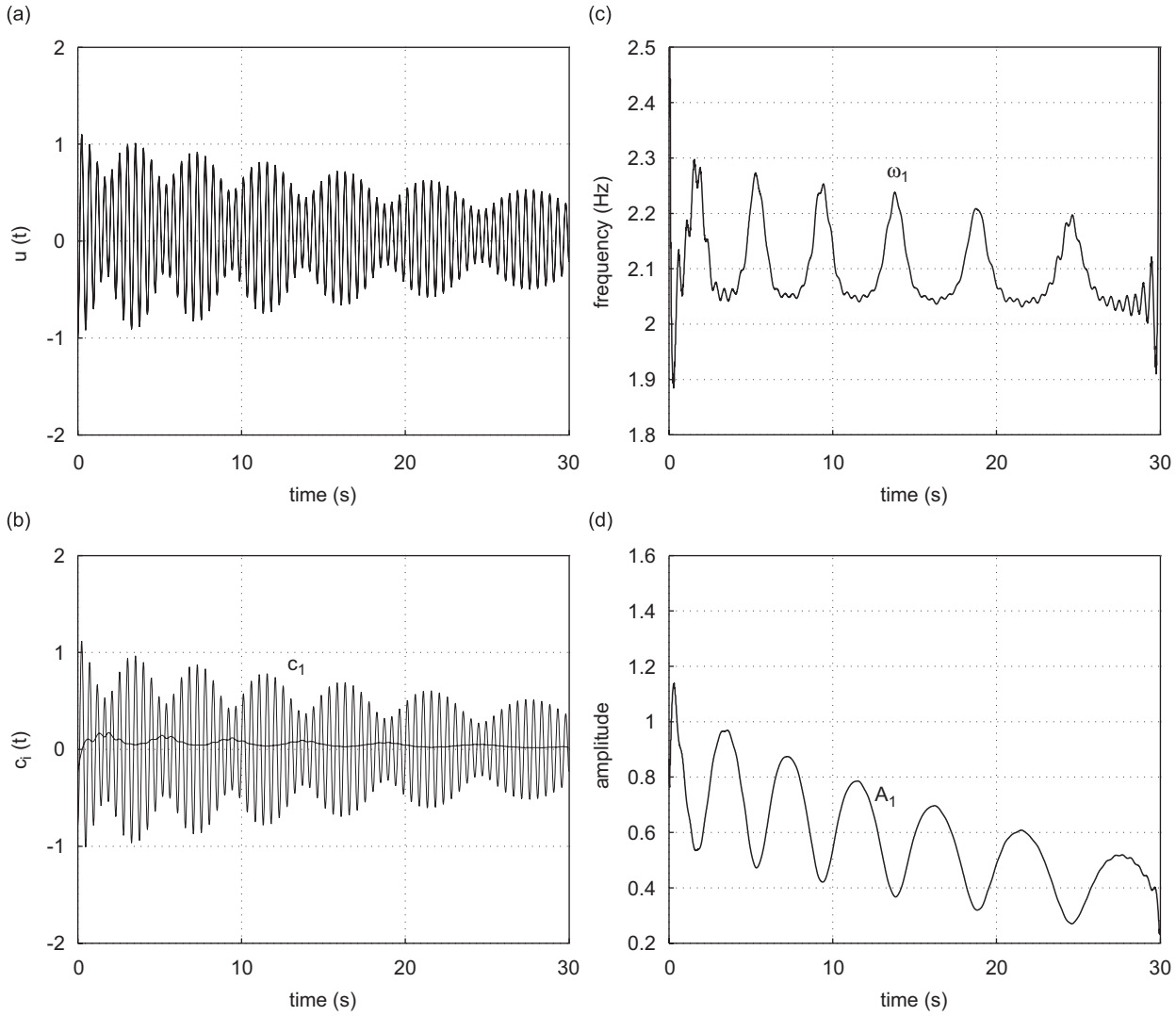

Fig. 10. Hilbert–Huang transform analysis of $u(t)$ $(= u_2(t))$ of Eq. (28): (a) $u_2(t)$, (b) c_1 and r_1, (c) ω_1 of c_1, and (d) A_1 of c_1.

data into components of different time scales and extracting detailed time-varying frequencies and amplitudes to reveal nonlinear characteristics of the data. Numerically a frequency tracking problem is somewhat more complicated than a system identification problem because less data are available for accurate estimation.

4. Concluding remarks

Methods of using the Hilbert–Huang transform and a sliding-window fitting method to extract nonlinear effects from nonlinear/non-stationary time signals are presented. Intrawave amplitude- and frequency-modulation explains the distortion of harmonic waves by nonlinear effects, and interwave amplitude- and frequency-modulation explains modal coupling of modes with different time scales. Major nonlinear phenomena that can be extracted from transient and/or steady-state dynamic responses include quadratic, cubic, and higher-order nonlinearities, softening and hardening effects, intrawave amplitude- and phase-modulated motions, distorted harmonic responses under a single-frequency harmonic excitation, interwave amplitude- and phase-modulated motions, and multiple-mode vibrations caused by internal/external

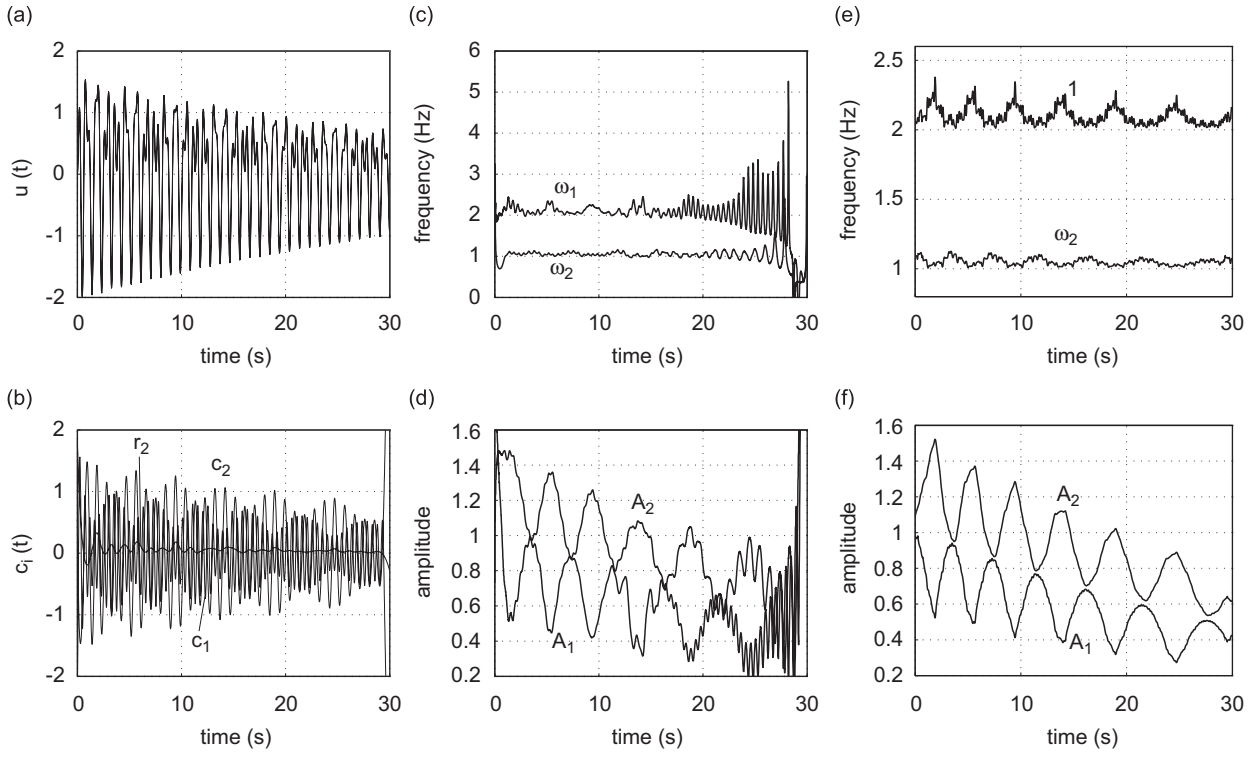

Fig. 11. Hilbert–Huang transform and sliding-window fitting analyses of $u(t)$ $(= u_1(t) + u_2(t))$ of Eq. (28): (a) $u_1 + u_2$, (b) c_i and r_2, (c) ω_i of c_i, and (d) A_i of c_i from Hilbert–Huang transform, (e) ω_i of c_i, and (f) A_i of C_i from sliding-window fitting.

resonances. The discontinuity-induced Gibbs' phenomenon at data ends in Hilbert–Huang transform analysis needs further study in order to improve the accuracy and robustness.

Acknowledgements

This work is supported by the National Science Foundation through Grants CMS-0120798 and CMS-0319853 and the NASA Langley Research Center through Grant NAG-1-01037. The support is gratefully acknowledged.

References

[1] S.W. Doebling, C.R. Farrar, M.B. Prime, D.W. Shevitz, Damage identification and health monitoring of structural and mechanical systems from changes in their vibration characteristics: a literature review, Report No. LA-13070-MS, Los Alamos National Laboratory, 1996.

[2] P.F. Pai, B.S. Kim, J.H. Chung, Dynamics-based damage inspection of an aircraft wing panel, *Journal of Intelligent Material Systems and Structures* 15 (2004) 803–821.

[3] A.H. Nayfeh, D.T. Mook, *Nonlinear Oscillations*, Wiley, New York, 1979.

[4] A.H. Nayfeh, P.F. Pai, *Linear and Nonlinear Structural Mechanics*, Wiley-Interscience, New York, 2004.

[5] A.H. Nayfeh, *Introduction to Perturbation Techniques*, Wiley-Interscience, New York, 1981.

[6] N.E. Huang, Z. Shen, S.R. Long, M.C. Wu, H.H. Shih, Q. Zheng, N.C. Yen, C.C. Tung, H.H. Liu, The empirical mode decomposition and the Hilbert spectrum for nonlinear and non-stationary time series analysis, *Proceedings of the Royal Society of London Series A—Mathematical Physical and Engineering Sciences* 454 (1998) 903–995.

[7] N.E. Huang, Z. Shen, S.R. Long, A new view of nonlinear water waves: the Hilbert spectrum, *Annual Reviews of Fluid Mechanics* 31 (1999) 417–457.

[8] N.E. Huang, M.C. Wu, S.R. Long, S.S.P. Shen, W. Qu, P. Gloersen, K.L. Fan, A confidence limit for the empirical mode decomposition and Hilbert spectral analysis, *Proceedings of the Royal Society of London Series A—Mathematical Physical and Engineering Sciences* 459 (2003) 2317–2345.

[9] Z. Wu, N.E. Huang, A study of the characteristics of white noise using the empirical mode decomposition method, *Proceedings of the Royal Society of London Series A—Mathematical Physical and Engineering Sciences* 460 (2004) 1597–1611.
[10] N.E. Huang, N.O. Attoh-Okine (Eds.), *The Hilbert–Huang Transform in Engineering*, CRC Press, Boca Raton, FL, 2005.
[11] E.O. Brigham, *The Fast Fourier Transform*, Prentice-Hall, Englewood Cliffs, NJ, 1974.
[12] G. Strang, T. Nguyen, *Wavelets and Filter Banks*, Wellesley-Cambridge Press, Wellesley, MA, 1997.
[13] P. Flandrin, *Time–Frequency/Time-Scale Analysis*, Academic Press, New York, 1999.
[14] P.F. Pai, L. Huang, Hilbert–Huang decomposition of time signals for structural damage detection, *SPIE 11th Annual Symposium on NDE for Health Monitoring and Diagnostics*, San Diego, California, February 26–March 2, 2006.